Asian Journal of Chemistry; Vol. 33, No. 1 (2021), 76-82

ASIAN JOURNAL OF CHEMISTRY

https://doi.org/10.14233/ajchem.2021.22943

Development of Chitosan-Collagen/Substituted Hydroxyapatite-Polypyrrole Biocomposite with Prospective Application in Bone Tissue Engineering Scaffolds

P. LAVANYA[1,2,*], N. VIJAYAKUMARI[1,*], R. SANGEETHA[1,3] and G. PRIYA[1,3]

[1]Department of Chemistry, Government Arts College for Women, Salem-636008, India
[2]Department of Chemistry, Vivekanandha College for Arts and Science for Women, Veerachipalayam, Sankari-637303, India
[3]Department of Chemistry, Shri Sakthikailassh Women's College, Salem-636003, India

*Corresponding author: E-mail: srilavs870@gmail.com

Received: 14 August 2020; *Accepted*: 21 September 2020; *Published online*: 10 December 2020; AJC-20180

An innovative hybrid based on chitosan-collagen/copper, manganese substituted hydroxyapatite-polypyrrole (CS-COL/CMHA-PPY) was developed in present study to further enhance the surface morphology of regenerative medicine scaffolds by combining the synthesized copper, manganese substituted hydroxyapatite (CMHA) and polypyrrole with the chitosan and collage solution accompanied by solvent casting techniques. The fabricated biocomposite was characterized using FTIR, XRD and SEM techniques. It investigated the effects of CMHA and polypyrrole on the scaffold's physico-chemical characteristics like swelling proportion, degradation, and mechanical nature. The CS-COL/CMHA-PPY biocomposite demonstrated lower deterioration rate and higher mechanical properties according to the chitosan-collagen and CS-COL/CMHA biocomposite. MTT assay conducted a tentative evaluation of the tissue engineering and cytotoxicity of the chitosan-biocomposite scaffold utilizing osteoblast cells. Tests demonstrated no toxicity, so osteoblast cells were bound to the biocomposite pore surfaces so propagated. Such results indicated that the scaffold established has the preconditions which can be used as a scaffold for the reconstruction of bone tissue.

Keywords: Bone, Composite, Polypyrrole, Scaffolds, Tissue engineering.

INTRODUCTION

Regenerative medicine focuses on the restoration of defective or defective muscle cells and includes three essential elements: biomaterials, immune cells, and the origins of cells [1]. Biomaterials are important in this pathway to tissue replication, because it acts as three-dimensional scaffolds which provide complex impacts and help for cell growth and division to develop a massive tissue. A scaffold will imitate the actual extracellular matrix (ECM) condition of engineered tissue to facilitate successful tissue repair and facilitate the production of accordion-specific functions and cellular proliferation [2]. Different polymers for use in scaffolds for bone tissue engineering have been undertaken. Nevertheless, natural polymers including polysaccharides and proteins have strong biomechanical properties. Type I collagen is one of the genetically identical biomaterials and is more commonly utilized. Higher temperatures at biological ionic pressure and normal pH cause spontaneous formation into natural fibrils of type I collagen molecules [3]. The concurrent obtaining of collagen fibril arrangement and hydroxyapatite blend from the stock arrangements at unbiased or soluble base condition is an overall methodology to create collagen bone uniting biocomposites, and this methodology is additionally pertinent to some collagen-based natural frameworks for creating tissue designing platforms or multi-segment biocomposites. Chitosan is produced from *N*-deacetylated chitin, which actually resided in the exoskeleton of arthropods, and was commonly used for biomedical applications [4]. In acidic conditions, it is dissolved by protonation and mixed by collagen.

In tissue engineering, a large range of products is used to improve the mechanical strength and biocompatibility of polymers in scaffold matrices. The application of polymer items with hydroxyapatite to bone regenerative medicine may be valuable [5]. Notably, hydroxyapatite (HA) imitates the HA crystals in humans including teeth and bones, has been used to trigger a

substantially enhanced protein uptake and cell attachment. With the introduction of ionic substitutions like cations and anions, the physico-chemical and biological characteristics of hydroxyapatite are enhanced. Copper takes on a crucial role in human metabolism as the second most important trace factor of a human psyche [6]. Copper may promote the production of epithelial vascular endothelial cells which are useful for angiogenesis. Manganese is necessary for bone growth and improvement, while Mn insufficiency-induce delayed osteogenic differentiation that causes bone defects [7]. Copper and manganese as essential nutrients ions will also play a crucial position in the enhancement of hydroxyapatite biocompatibility and antibacterial action for medical applications [8].

In addition to biomaterials, recently conducted polymers are of importance to biomedical technology, as emerging technologies may need biotechnology that not only mechanically help tissue development, but are also electroactive and can, therefore, stimulate different cellular activities or activate immune response [9]. Polypyrrole is the most desirable conductive polymers and may ultimately be used in biological devices. Such conductive materials also exhibit strong *in vitro* and *in vivo* bioactivity [9]. Researches on cells grown on the conduction of polymer substrates results showed favorable cellular impact in promoting and modifying certain types of regenerative medicine, such as tendon, skin, cardiovascular myofibroblasts, skeletal muscle and skeletal muscles [10]. This research aimed to create an innovative biocomposite and test its possible use as a bone restoration scaffold. Biocomposite scaffolds were formulated using the solvent casting method based on chitosan (CS), collagen (COL), copper, manganese substituted hydroxyapatite (CMHA) and polypyrrole (PPY) and extensively examined by FT-IR, XRD, SEM, swelling, degradation and mechanical evaluations. Antibacterial activity, hemocompatibility and MTT assay studies on these biocomposite scaffolds were also conducted.

EXPERIMENTAL

Preparation of CMHA nanoparticles: In brief, for the synthesis of CMHA nanoparticles, solutions of calcium (0.9 M), copper (0.05 M), manganese (0.05 M), and 0.6 M $(NH_4)_2HPO_4$ were individually adjusted to pH 9 to 10 *via* using NaOH solution. A solution of $(NH_4)_2HPO_4$ was slowly mixed into the formulation of the mineral (calcium, copper and manganese) to create a colloidal dispersion. The solution was agitated at 600 rpm for 12 h, accompanied by precipitation aging for 1 day. The precipitates collected was soaked with demineralized water several times and then separated by centrifugation. The material was dried in the oven at 100 ºC and sintered at 800 ºC for 5 h.

Preparation of biocomposite: Hybrid biocomposites based on chitosan-collagen (CS-COL), chitosan, collagen, copper, manganese substituted hydroxyapatite (CS-COL-CMHA) and chitosan, collagen, copper, manganese substituted hydroxyapatite and polypyrrole (CS-COL-CMHA-PPY) were developed using a basic blending process. Chitosan-collagen biocomposite (CS-COL) were fabricated according to the procedure described earlier [11]. Then, CMHA (10% wt.) was distributed in acetic acid medium (1% v/v) for 12 h and this mixture was introduced to the agitated CS-COL solution for 12 h. Polypyrrole (PPY) (1% wt.) was then distributed in acetic acid medium (1% v/v) for 24 h and then experienced with soni-cation and applied to the CS-COL/CMHA suspension through agitation for 12 h. The CS-COL/CMHA-PPY biocomposite solution was consequently casted on the glass plate and dried the films at 37 ºC for 3 days. Resulting CS-COL/CMHA-PPY biocomposite also were treated with NaOH solution (1% v/v) to extract excessive acetic acid and washed with sufficient demineralized and casted again. Similar techniques were used to construct CS-COL/CMHA biocomposite for contrast with CS-COL/CMHA biocomposite.

Characterization: X-ray diffraction spectrometry was obtained using CuKα radiation with XRD (DX-2000). The FTIR spectra are measured with a NICOLET 200SXV Infrared Spectrophotometer at room temperature. SEM (JSM-5900LV, JEOL) has done the morphological characterization of the biocomposite. A TEM (H-6009IV, Hitachi) was conducted for the morphological characterization of CMHA. The biocomposite material characteristics have been assessed and use a testing machine (AI-7000-M, Gotech Testing Machine Inc).

Swelling studies: For swelling study, the biocomposite was brooded in demineralized water at room temperature. At that point, tests were taken out and gauged after delicate surface cleaning with permeable paper at a normal time frame until balance growing was reached. The equilibrium swelling ratio (SR) is characterized as the proportion of swollen load to the underlying weight. To limit the test blunder, all the investigations were acted in triplicate and their normal worth was recorded [12].

Biodegradation: The biodegradation of the biocomposite platforms was concentrated in PBS enclosing lysozyme at room temperature. Biocomposite was submerged in PBS and hatched at room temperature for 7, 14 and 21 days. Introductory loads of the biocomposite was marked as W_o and after inundation, the biocomposite were washed in refined water to evacuate the surface adsorbed particles and casting [13].

Antimicrobial activity: The antimicrobial movement was assessed by the development hindrance examine utilizing the technique clarified somewhere else [14].

Alkaline phosphatase (ALP) activity: Osteogenic separation of the bone cells was surveyed by ALP. The ALP assay procedure was adopted from an earlier report [15].

Measurement of cytotoxicity: The biocompatibility of biocomposite was evaluated by deciding the suitability of the MG-63 osteoblast cells because of the molded media utilizing MTT measures. Quickly, biocomposite plates were cleaned in 70% ethanol followed by washing in a sterile PBS. Osteoblast cells were seeded on the biocomposite surface in a 96-well plate with DMEM enhanced with 10% FBS and brooded at room temperature for 3 days in 5% CO_2. Subsequently, the solution was supplanted with MTT and hatch for another 5 h. At long last, 100 µL of DMSO was included with delicate blending in a shaker. The cell culture medium with no treatment was considered as control [16].

Statistics: Every quantitative outcome was acquired from triplicate tests and the results were evaluated as a mean ± standard deviation.

RESULTS AND DISCUSSION

Characterization CMHA nanoparticles: Meanwhile, P-O stretching asymmetric adsorption from phosphate functional group at 1150-1000 cm^{-1} is seen in the FTIR spectrum, which is classified as apatite peak attributes, and a medium strength peak was examined at around 910 cm^{-1} attributable to symmetric stretching vibration [17]. A peak at 620-560 cm^{-1} detected the bending frequency of the phosphate functional group. Similarly, the phosphate extending asymmetric and medium amplitude was observed at 1022 and 962 cm^{-1}, independently. Another peaks at 3540 and 620 cm^{-1} refer to the hydroxyl group [17] (Fig. 1a).

XRD studies: The usual XRD patterns of all the specimens display a hexagonal hydroxyapatite phase structure; in strong accordance with approved data (JCPDS card No. 09-0432) [18]. Significant diffraction peaks are found at two theta values of 32º, 31º and 25º referred to (300), (211), (211) and (201) crystal planes, respectively [19]. The development of major peak diffraction shows the productive data of the specimens being processed (Fig.1b). The XRD spectral data collected during the current examination are all in fair accordance with the reported values. Therefore, the findings for the XRD are in strong alignment with the results for FTIR analysis.

Morphologies studies: Fig. 1c displays the SEM image of the prepared CMHA nanoparticles. The structure of particles is in the nano-rod configuration. The path of crystal growth indicated some of the identified aggregation in the final products. It seems to be that the sizes of the particles are homogenous all around, showing a high crystalline structure of the particles. Fig. 1d demonstrate the microscopic examination (TEM) of the produced CMHA nanoparticles. The intensity of the particle surfaces in these crystalline structure is incredibly high.

Characterization biocomposite: FTIR spectra of CS/COL, CS/COL/CMHA and CS/COL/CMHA-PPY biocomposites are shown in Fig. 2a. The FTIR spectroscopy of all biocomposite

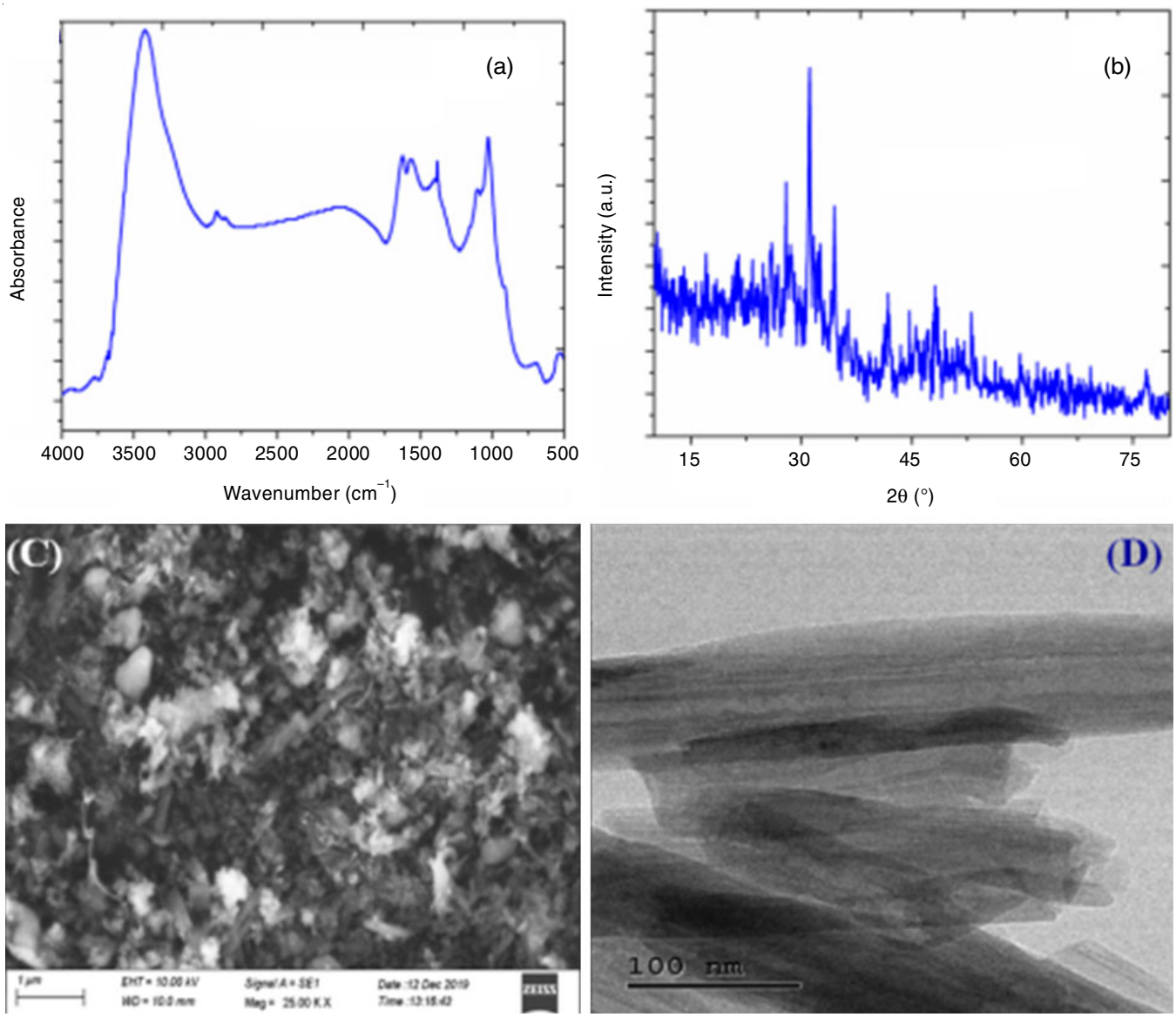

Fig. 1. FTIR spectra (a), X-ray diffraction spectra (b), SEM (c) and TEM (d) of prepared CMHA nanoparticles

materials display a peak at roughly 1400-1200, 1600-1500 and 1700-1600 cm^{-1} attributed due to amides I, II and III, respectively [20,21]. Absorption of amide-I is attributed to C=O vibration stretching and amide- II absorption is attributed to twisting motions of amide N-H and C-N vibration stretching of vibration. A peak of amide-III is complexed due to the involvement of a portion of C-N asymmetric stretching from amide group and stretching vibrations from the methyl units of glycine spine and proline side groups. A broad peak at ~3500-3000 cm^{-1} suggested the vibrations of N-H and O-H stretching. A peak at 2940-2860 cm^{-1} was examined with the symmetric C-H stretching vibration characteristic to pyranose moiety [21]. The peaks owed to the stretching vibration of C-O at ~ 1077-1070 cm^{-1}. The phosphate group absorption peaks detected at 1100-1000 cm^{-1} indicating the presence of CMHA nanoparticles [22]. The CS-COL/CMHA-PPY biocomposite does not exhibit no clear bands change from CS-COL/CMHA despite the existence of pyrrole ring groups C-C (1521 cm^{-1}), C-N (1625 cm^{-1}) and N-H (3400 cm^{-1}) [21]. In these findings, it can be inferred that the PPY loaded with CS-COL/CMHA was effectively inserted into the biocomposite.

As seen in Fig 2b, CS-COL/CMHA-PPY composite and CS-COL/CMHA have identical XRD profiles. Almost all the diffraction patterns are well described and allocated to the crystal structure monophase. The CMHA mainly, while no peaks of other calcium and phosphate components are observed. It shows that the presence of chitosan, collagen and polypyrrole did not altered the crystalline structure composition of CMHA nanoparticles in the biocomposite. The CS-COL/CMHA-PPY and CS-COL/CMHA biocomposite diffraction plane are significantly larger than CMHA, which is an indication of reduced CMHA crystal structure despite the existence of a polymer network. While the signature diffractions plane of CMHA is found at 002 (26º), 211 (31º), 310 (39º) for biocomposites (Fig. 2b) [23]. This shift suggests that hydroxyapatite preparation prevented the crystal structure of the polymeric material in the co-precipitation cycle, in compliance with earlier studies [24].

The appropriate surface morphology of the pores is the main factor for efficient scaffolding, which involves porous depth, permeability, pore-to-pore connectivity, and surface-to-volume proportion. Biocomposite scaffoldings should be extremely porous with sufficient pore volume to promote cell replication, cell growth and tissue formation far within the pores and porous to encourage the development of arteries, the transfer of vitamins and minerals and the elimination of waste products [25]. The SEM results of the prepared CMHA and PPY and the prepared hybrid scaffolding (CS-COL, CS-COL/CMHA and CS-COL/CMHA-PPY) are shown in Fig. 2c-e. The ensuing porous biocomposite scaffolds had hierarchical porous materials with well-connected pores. The pore depth of the CS-COL biocomposite was roughly 150-300 µm (Fig. 2c). Throughout the CS-COL/CMHA biocomposite, the CMHA nanoparticles were randomly scattered on the surfaces of the biocomposite. The porous depth of CS-COL/CMHA biocomposite ranges from 150-300 µm as determined by SEM (Fig. 2d). The average pore volume of the CS-COL/CMHA-PPY biocomposite has been estimated to be 150 µm (Fig. 2e). The intro-

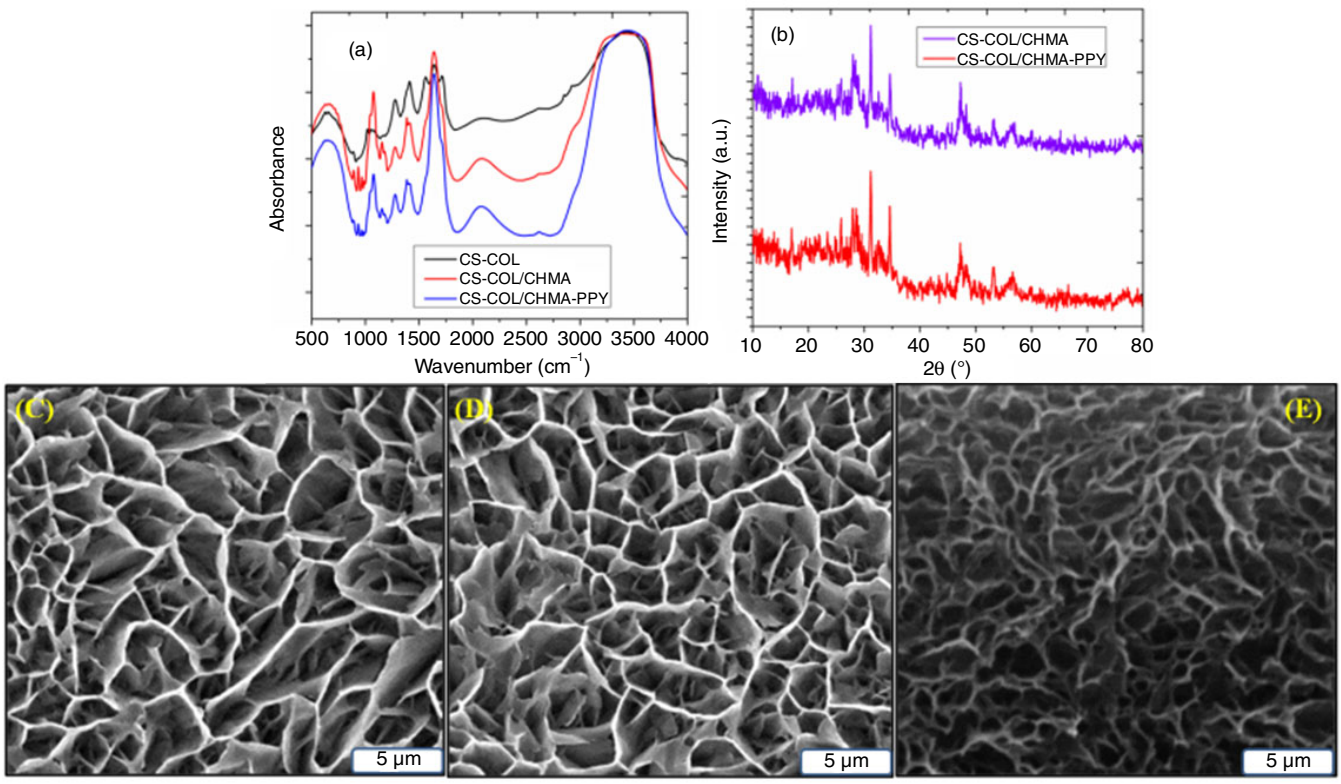

Fig. 2. (a) FTIR spectra (b) X-ray diffraction spectra of prepared samples. SEM images of (c) CS-COL, (d) CS-COL/CMHA and (e) CS-COL/CMHA-PPY biocomposites

duction of polypyrrole has been seen to reduce the pore size of the scaffold and even the porous form has been asymmetrical.

Mechanical properties: Although biocomposite scaffolds are supposed to fail after *in vivo* implantation, around for scaffolds to survive a certain amount of biochemical loading a certain degree of mechanical properties is needed [26]. The CS-COL, CS-COL/CMHA and CS-COL/CMHA-PPY biocomposites were tested with their mechanical properties (compressive and tensile properties) (Table-1). When contrast to the CS-COL, the ultimate tensile of CS-COL/CMHA, a scaffold was weaker. Adding polypyrrole to the CS-COL/CMHA matrix therefore improved its tensile capacity. Through inserting CMHA into the CS-COL scaffold the compressive power of the CS-COL/CMHA reduced. The CS-COL/CMHA compressive intensity was just 3410 KPa while the CS-COL compressive strength was 4120 KPa. The addition of CMHA, which is more fragile than CS-COL, undoubtedly improved the ductility of hybrid biocomposites from CS-COL/CMHA, resulted in a subsequent reduction in their compressive power. In addition, accumulation of CMHA crystals may arise in biocomposite scaffolds with CS-COL/CMHA. Because of the poor contact between CMHA and CS-COL matrix, broader CMHA crystals serve as fractures in the persistent chitosan-gel matrix. Furthermore, the addition of polypyrrole into CS-COL/CMHA network improved the scaffold′s compressive power. The CS-COL/CMHA-PPY biocomposite had a compressive power of 5235 kPa. The application of polypyrrole in the CS-COL/CMHA network with a standardized spread may increase the tensile stability of the scaffold. In fact, reduced permeability of scaffolds and improved density of porous walls significantly influence the mechanical properties.

TABLE-1
MECHANICAL PROPERTIES OF THE BIOCOMPOSITE

Samples	Tensile strength (MPa)	Young modulus (KPa)	Compressive strength (KPa)
CS-COL	0.650	17666	4120
CS-COL/CMHA	0.436	16375	3410
CS-COL/CMHA-PPY	1.321	26258	5235

Swelling studies: The capacity to swell is a significant metric for the scaffolds in their bone tissue engineering. Swelling capacity is highly essential for body absorption [27]. The biocomposite medium absorption potential was measured by assessing the composite swelling ratio in phosphate buffer solution at room temperature. The consequence revealed that combining CMHA-PPY with CS-COL reduced the biocomposite swelling capacity, which might be due to the hydrophobic feature of polypyrrole. Nevertheless, the biocomposite formed indicates an improvement in swelling and therefore encourages cell penetration into the biocomposite. Several hydrophilic classes of macromolecules were also concerned owing to contact with polymer chains, CMHA and polypyrrole, and the solvent absorption was reduced, which minimized the swelling (Fig. 3a). Diminishing swelling behaviour may influence the mechanical characteristics of scaffolds. In other words, using adequate amounts of materials in the scaffold matrix, the water uptake and swelling can be regulated [28].

***in vitro* Degradation studies:** Since regenerative medicine aims at stimulating fresh tissues, it is anticipated that the scaffolds should be biodegradable and absorbable at a suitable pace to suit the level of development of fresh tissues [29]. The degradation activity of biocomposite plays a significant part in the development phase of a fresh tissue in physiologic conditions. Fig. 3b demonstrates the efficiency of CS-COL, CS-COL/CMHA and CS-COL/CMHA-PPY biocomposite scaffolds in PBS-containing lysozyme *in vitro* bioremediation. The procedure of degradation involves hydrolyzing collagen and enzymatic biodegradation by chitosan. The analysis thus portrays the biodegradability and resilience of the biocomposite formed under the biological system.

Antibacterial activity: Current emphasis of present study was on to synthesize bicomposite that impart antibacterial activity through the introduction of polypyrrole and thus the antibacterial behaviour of CS-COL/CMHA-PPY bicomposite against CS-COL/CMHA bicomposite for the zone of inhibition (ZOI) towards Gram-negative (*E. coli*) and Gram-positive (*S. aureus*) bacterial strains were measured (Fig. 4a). The ZOI of the CS-COL/CMHA-PPY bicomposite was found to be 14.78

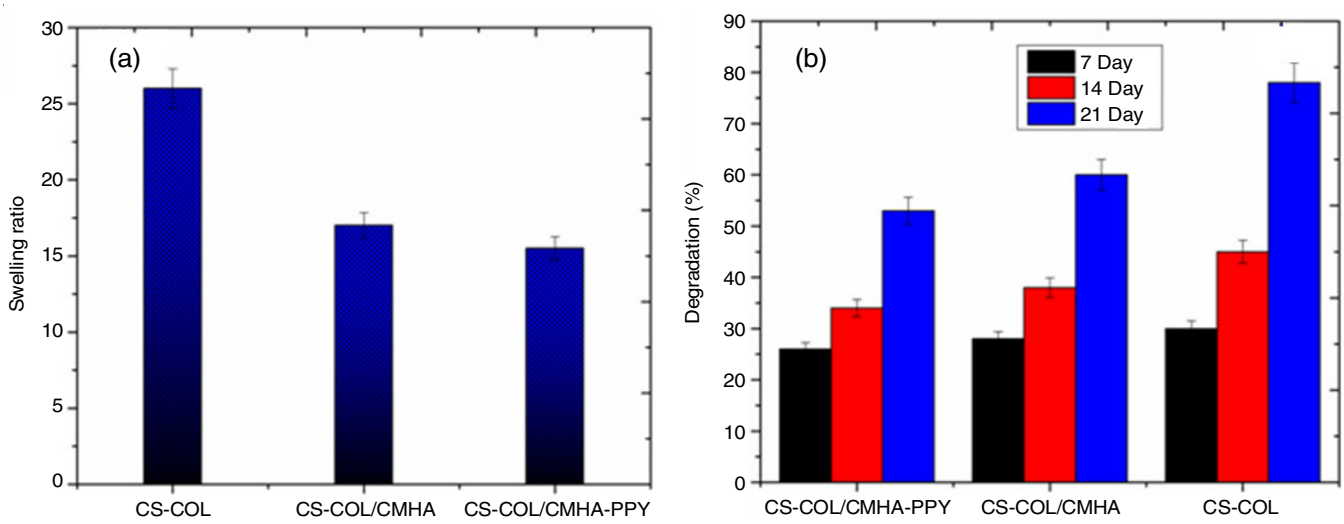

Fig. 3. Swelling behaviour (a) and biodegradation of biocomposite (b)

± 3.55 mm and 12.34 ± 2.50 mm against *E. coli* and *S. aureus*, respectively. The CS-COL and CS-COL/CMHA biocomposites ZOI against *E. coli* and *S. aureus* was considerably low which may be attributed to the existence of chitosan, copper and manganese that has normal antibacterial efficacy [30,31]. The results indicated that the greater inhibition zone for CS-COL/CMHA-PPY biocomposite was attributed to polypyrrole antibacterial function [31]. Therefore, the biocomposite CS-COL/CMHA-polypyrrole have a wide range of bactericidal activityagainst *E. coli* and *S. aureus*.

Hemolytic assay: To test the blood compatibility of prepared biocomposite, an *in vitro* hemocompatibility assay was conducted. When a scaffold material is placed inside, it initiates numerous different *in vivo* encounters and there is ionic exchange, which can cause lysis to scratch the blood cells [32]. The fabricated biocomposite had to be tested for its contact with the bloodstream to avoid lysis of the blood cells. The results of the hemolytic assay confirmed the viability of CS-COL and CS-COL/CMHA with blood, as the hemolysis for each of these biocomposite membranes was lower than 5% (Fig. 4b). These results show that the minimal doses of adding polypyrrole had no adverse effects on human erythrocytes. Such values are relatively below which are reported earlier [33].

Alkaline phosphatase (ALP) activity: Alkaline phosphatase (ALP) activity is a precursor of osteogenic proliferation and bony recovery mineralization, an elevated alkaline activity indicates extracellular matrix functions [34]. Regarding the ALP activity of the CS-COL, CS-COL/CMHA membranes of the osteoblast cells, it is found that the CS-COL/CMHA-PPY bicomposite had a greater ALP expression on the 3rd and 7th day after preliminary implantation than CS-COL bicomposite (Fig. 4c). The elevated behaviour can be due in CS-COL/CMHA-PPY to the existence of polypyrrole. The general pattern in day 3 to day 7 ALP behaviour confirms that there is an improvement in CS-COL/CMHA-PPY osteogenic capacity over CS-COL, likely because of the introduction of polypyrrole. The several studies indicated that polypyrrole nanoparticles encourage behaviour in ALP [35,36]. Also, Hardy *et al.* [37] stated that the polypyrrole loaded nanofiber issued by the competent ALP behaviour instead of using the electrical stimulation or osteogenic medium.

A tentative assessment of the cytocompatibility of CS-COL, CS-COL/CMHA and CS-COL/CMHA-PPY scaffolds was also carried out by MTT assay in the proposed work. Fig. 5a indicates biocompatibility of osteoblast cell lines with CS-COL, CS-COL/CMHA and CS-COL/CMHA-PPY biocomposite after 1, 2 and 3 days incubation. After 3rd day of treatment, all biocomposite endorsed cell feasibility of 80-100% for osteoblast cell lines, indicating strong cell viability and cytocompatibility. Consistent with existing research, it can be inferred that the PPY-containing CS-COL/CMHA-PPY biocomposite as a conducting polymer exhibited total low toxic results *ex vivo* and its effects can also be regulated by the synergetic action of CMHA and polypyrrole. The bioactivity of the biocom-

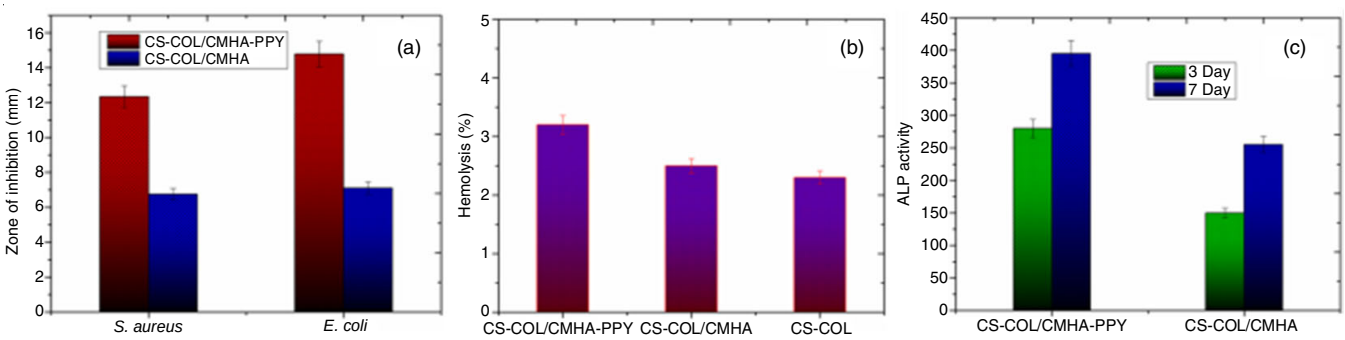

Fig. 4. Antibacterial activity (a), hemocompatibility (b) and ALP activity (c) of prepared samples

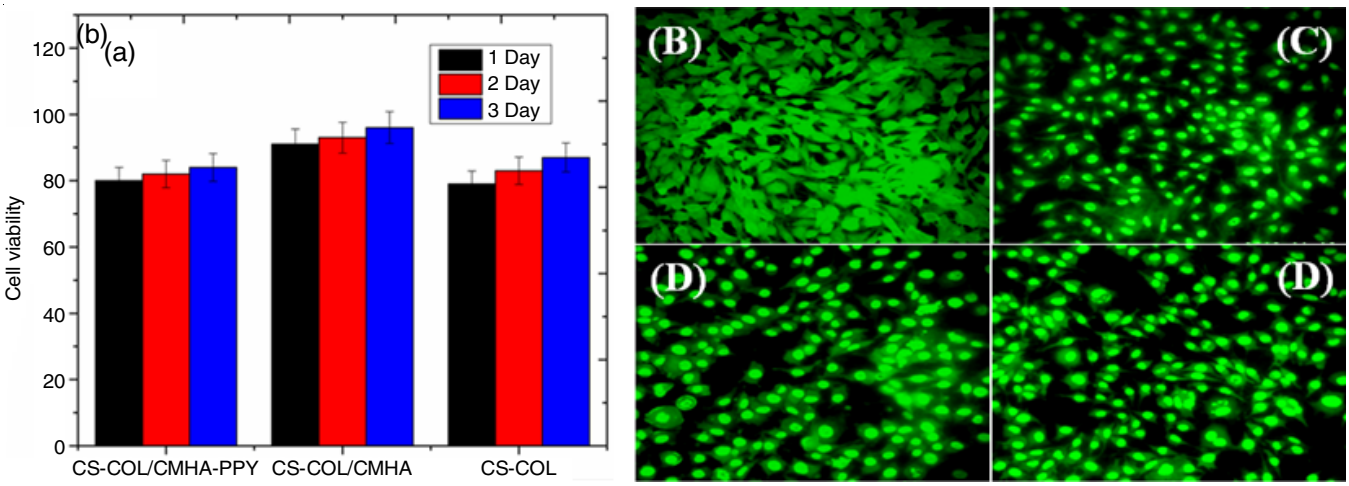

Fig. 5. Osteoblast cell viability (a), and live dead cell assay on biocomposite towards CS-COL (b), CS-COL-CMHA (c), and CS-COL/CMHA-PPY (d) biocomposites samples after 3rd day culture

posite established was further verified by live/dead staining assay (Fig. 5b-e) after 3rd day incubation.

Conclusion

In this study, a solvent casting approach was used to construct 3D chitosan-collagen/copper, manganese substituted hydroxyapatite-polypyrrole (CS-COL/CMHA-PPY) for biomedical applications. The characterization of the biocomposite was based on FT-IR, XRD and SEM techniques. The physical characteristics of CS-COL/CMHA-PPY biocomposite were contrasted with the respective CS-COL and CS-COL/CMHA biocomposite and studied the adaptive impact of CMHA and polypyrrole. Through applying polypyrrole to biocomposite matrix, it is possible to regulate the biocomposite characteristics such as swelling, degradation and mechanical activities. Studies on cytocompatibility and live/dead cell assay have shown that the designed biocmposite is biocompatible to the cell lines osteoblast. Such experiments showed that CS-COL/CMHA-PPY biocomposite may be a successful choice for restoration of bone tissue.

CONFLICT OF INTEREST

The authors declare that there is no conflict of interests regarding the publication of this article.

REFERENCES

1. G.S. Hussey, J.L. Dziki and S.F. Badylak, *Nat. Rev. Mater.*, **3**, 159 (2018); https://doi.org/10.1038/s41578-018-0023-x
2. M. Walraven and B. Hinz, *Matrix Biol.*, **71-72**, 205 (2018); https://doi.org/10.1016/j.matbio.2018.02.020
3. W. Friess, *Eur. J. Pharm. Biopharm.*, **45**, 113 (1998); https://doi.org/10.1016/S0939-6411(98)00017-4
4. K. Kalantari, A.M. Afifi, H. Jahangirian and T.J. Webster, *Carbohydr. Polym.*, **207**, 588 (2019); https://doi.org/10.1016/j.carbpol.2018.12.011
5. K. Aoki and N. Saito, *Pharmaceutics*, **12**, 95 (2020); https://doi.org/10.3390/pharmaceutics12020095
6. R. Ghosh, O. Swart, S. Westgate, B.L. Miller and M.Z. Yates, *Langmuir*, **35**, 5957 (2019); https://doi.org/10.1021/acs.langmuir.9b00919
7. S. Kandasamy, V. Narayanan and S. Sumathi, *Int. J. Biol. Macromol.*, **145**, 1018 (2020); https://doi.org/10.1016/j.ijbiomac.2019.09.193
8. T. Tite, A.C. Popa, L.M. Balescu, I.M. Bogdan, I. Pasuk, J.M. Ferreira and G.E. Stan, *Materials*, **11**, 2081 (2018); https://doi.org/10.3390/ma11112081
9. B. Guo, L. Glavas and A.C. Albertsson, *Prog. Polym. Sci.*, **38**, 1263 (2013); https://doi.org/10.1016/j.progpolymsci.2013.06.003
10. A. Talebi, S. Labbaf and F. Karimzadeh, *Polym. Compos.*, **41**, 645 (2020); https://doi.org/10.1002/pc.25395
11. N. Thongtham, P. Chaiin, O. Unger, S. Boonrungsiman and O. Suwantong, *Polym. Adv. Technol.*, **31**, 1496 (2020); https://doi.org/10.1002/pat.4879
12. M.F. Abou Taleb, A. Alkahtani and S.K. Mohamed, *Polym. Bull.*, **72**, 725 (2015); https://doi.org/10.1007/s00289-015-1301-z
13. J. Venkatesan, R. Pallela, I. Bhatnagar and S.-K. Kim, *Int. J. Biol. Macromol.*, **51**, 1033 (2012); https://doi.org/10.1016/j.ijbiomac.2012.08.020
14. Y.S. Wei, K.S. Chen and L.T. Wu, *J. Inorg. Biochem.*, **164**, 17 (2016); https://doi.org/10.1016/j.jinorgbio.2016.08.007
15. R. Jolly, A.A. Khan, S.S. Ahmed, S. Alam, S. Kazmi, M. Owais, M.A. Farooqi and M. Shakir, *Mater. Sci. Eng. C*, **109**, 110554 (2020); https://doi.org/10.1016/j.msec.2019.110554
16. J. Zhang, G. Liu, Q. Wu, J. Zuo, Y. Qin and J. Wang, *J. Bionics Eng.*, **9**, 243 (2012); https://doi.org/10.1016/S1672-6529(11)60117-0
17. J. Mobika, M. Rajkumar, V.N. Priya and S.P. Linto Sibi, *J. Mol. Struct.*, **1206**, 127739 (2020); https://doi.org/10.1016/j.molstruc.2020.127739
18. R. Sarkar, A. Agrawal and R. Ghosh, *Trans. Indian Ceram. Soc.*, **78**, 101 (2019); https://doi.org/10.1080/0371750X.2019.1619484
19. L. Sundarabharathi, D. Ponnamma, H. Parangusan, M. Chinnaswamy and M.A.A. Al-Maadeed, *SN Appl. Sci.*, **2**, 94 (2020); https://doi.org/10.1007/s42452-019-1807-3
20. S.F. Ivanova and N.N. Petrova, *Mater. Sci. Forum*, **945**, 422 (2019): https://doi.org/10.4028/www.scientific.net/MSF.945.422
21. K.P. Ananth, A.J. Nathanael, S.P. Jose, T.H. Oh and D. Mangalaraj, *Mater. Sci. Eng. C*, **59**, 1110 (2016); https://doi.org/10.1016/j.msec.2015.10.045
22. M. Catauro, F. Barrino, I. Blanco, S. Piccolella and S. Pacifico, *Coatings*, **10**, 203 (2020); https://doi.org/10.3390/coatings10030203
23. D. Luo, L. Sang, X. Wang, S. Xu and X. Li, *Mater. Lett.*, **65**, 2395 (2011); https://doi.org/10.1016/j.matlet.2011.05.011
24. L. Wang and C. Li, *Carbohydr. Polym.*, **68**, 740 (2007); https://doi.org/10.1016/j.carbpol.2006.08.010
25. M. Lee, R. Rizzo, F. Surman and M. Zenobi-Wong, *Chem. Rev.*, **120**, 10950 (2020); https://doi.org/10.1021/acs.chemrev.0c00077
26. R. Junka and X. Yu, *Mater. Sci. Eng. C*, **113**, 110981 (2020); https://doi.org/10.1016/j.msec.2020.110981
27. A. Sionkowska, A. Tuwalska, *Int. J. Polym. Anal. Charact.*, **25**, 315 (2020); https://doi.org/10.1080/1023666X.2020.1786271
28. V. Sencadas, S. Sadat and D.M. Silva, *J. Mech. Behav. Biomed. Mater.*, **102**, 103474 (2020); https://doi.org/10.1016/j.jmbbm.2019.103474
29. P. Datta, B. Ayan and I.T. Ozbolat, *Acta Biomater.*, **51**, 1 (2017); https://doi.org/10.1016/j.actbio.2017.01.035
30. M. Geraghty, J.F. Cronin, M. Devereux and M. McCann, *Biometals*, **13**, 1 (2000); https://doi.org/10.1023/A:1009271221684
31. A. Talebi, S. Labbaf and F. Karimzadeh, *Polym. Test.*, **75**, 254 (2019); https://doi.org/10.1016/j.polymertesting.2019.02.029
32. I. Denry and L.T. Kuhn, *Dent. Mater.*, **32**, 43 (2016); https://doi.org/10.1016/j.dental.2015.09.008
33. Y. Wu, Y. Wang, H. Chen, S. Ge, J. Zhang, C. Mao, H. Ding and J. Shen, *J. Nanosci. Nanotechnol.*, **16**, 2343 (2016); https://doi.org/10.1166/jnn.2016.10955
34. J. Liao, X. Guo, D. Nelson, F. Kurtis-Kasper and A.G. Mikos, *Acta Biomater.*, **6**, 2386 (2010); https://doi.org/10.1016/j.actbio.2010.01.011
35. A. Fahlgren, C. Bratengeier, A. Gelmi, C.M. Semeins, J. Klein-Nulend, E.W.H. Jager and A.D. Bakker, *PLoS One*, **10**, e0134023 (2015); https://doi.org/10.1371/journal.pone.0134023
36. H. Castano, E.A. O'Rear, P.S. McFetridge and V.I. Sikavitsas, *Macromol. Biosci.*, **4**, 785 (2004); https://doi.org/10.1002/mabi.200300123
37. J.G. Hardy, M.K. Villancio-Wolter, R.C. Sukhavasi, D.J. Mouser, D. Aguilar Jr., S.A. Geissler, D.L. Kaplan and C.E. Schmidt, *Macromol. Rapid Commun.*, **36**, 1884 (2015); https://doi.org/10.1002/marc.201500233